

Data augmentation for NeRF: a geometric consistent solution based on view morphing

Matteo Bortolon^{1,2,3} Alessio Del Bue² Fabio Poiesi^{1,2}

¹TeV, Fondazione Bruno Kessler ²PAVIS, Istituto Italiano di Tecnologia

³DISI, University of Trento
 {mbortolon, poiesi}@fbk.eu
 {alessio.delbue}@iit.it

Abstract

NeRF aims to learn a continuous neural scene representation by using a finite set of input images taken from different viewpoints. The fewer the number of viewpoints, the higher the likelihood of overfitting on them. This paper mitigates such limitation by presenting a novel data augmentation approach to generate geometrically consistent image transitions between viewpoints using view morphing. View morphing is a highly versatile technique that does not require any prior knowledge about the 3D scene because it is based on general principles of projective geometry. A key novelty of our method is to use the very same depths predicted by NeRF to generate the image transitions that are then added to NeRF training. We experimentally show that this procedure enables NeRF to improve the quality of its synthesised novel views in the case of datasets with few training viewpoints. We improve PSNR up to 1.8dB and 10.5dB when eight and four views are used for training, respectively. To the best of our knowledge, this is the first data augmentation strategy for NeRF that explicitly synthesises additional new input images to improve the model generalisation.

1 Introduction

Novel View Synthesis (NVS) is the problem of synthesising unseen camera views from a set of known views¹ [27, 7]. NVS is an enabling technology that can be used for augmented or virtual reality [9], entertainment [5], and robotics [10] applications. NVS has undergone a significant improvement after the introduction of Neural Radiance Fields (NeRF) [18, 1], which consists of a trainable implicit neural representation of a 3D scene that can photorealistically render unseen (novel) views. NeRF is typically trained with several images, e.g. about hundred images taken from different and uniformly distributed camera viewpoints around an object of interest [18]. If viewpoints are not uniformly distributed or they are few (e.g. four or eight), the resulting NeRF model may fail to produce satisfactory renderings [11, 17]. This is a practical problem that may occur when non-experts acquire images of an object in the wild [15] or when it is not possible to view objects from every side. When NeRF is trained on few and non-uniformly distributed viewpoints, the likelihood of overfitting on these viewpoints increases, namely the few-shot view synthesis problem [11]. Approaches that aim at addressing few-shot view synthesis include DietNeRF and pixelNeRF [11, 28]. The drawback of these methods is that they rely on auxiliary deep networks, which have to be trained on other datasets, thus requiring additional loss terms and increasing NeRF’s computational burden. Alternatively,

¹Throughout the paper, we will use the term *viewpoint* to refer to the camera pose, *view* to refer to the scene seen through a certain viewpoint and to *image* to refer to the photometric content captured from a view.

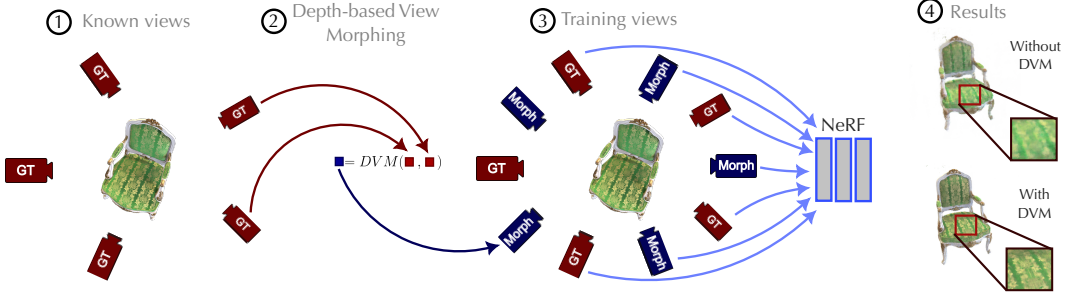


Figure 1: Given a set of (1) known views (ground truth), (2) our approach (DVM) generates image transitions between views (morph) that can be effectively used as data augmentation (3) to train a NeRF model in the case of few-shot view synthesis. (4) Results are of a higher quality when DVM is used.

data augmentation solutions can be used to mitigate overfitting [24], however they have not yet been explored for few-shot view synthesis.

In this paper, we propose a geometry-based data augmentation strategy that enables NeRF to efficiently learn implicit representations of scenes captured from few viewpoints. We reformulate the *view morphing* technique [23] to operate alongside NeRF. View morphing allows conventional image morphing methods to synthesise in-between viewpoint changes while ensuring realistic image transitions. View morphing does not require any prior knowledge about the captured 3D scene, and it can synthesise 3D projective transformations (e.g. 3D rotations, translations, shears) of objects by operating entirely on the input images. Because view morphing requires a dense pixel correspondence map between viewpoint pairs, we exploit the depth predicted by NeRF to retrieve the disparity map (Fig. 1). We implement a modified version of the rectification algorithm proposed by Fusiello et al. [6] to rectify images and disparity maps that are used by the view morphing process. The in-between viewpoints are randomly sampled between each viewpoint pair to produce the morphed views for training NeRF. We evaluate our approach by using the dataset used in the original NeRF’s paper [18] and we show that PSNR improves up to 1.8dB and 10.5dB when eight and four views are used for training, respectively. We also compare our approach with DietNeRF [11] and AugNeRF [4], and show that our approach can produce higher-quality renderings.

To summarise, our contributions are:

- A novel and effective data augmentation technique for NeRF for few-shot view synthesis;
- A new view morphing technique based on the NeRF depth output, named DVM;
- We show that DVM enables NeRF to produce higher-quality rendered images.

2 Related work

3D scene synthesis can be solved either by using traditional 3D reconstruction techniques [21] or by adopting methods based on neural rendering [25]. Neural radiance fields (NeRF) is a recent neural rendering method that can learn a volumetric representation of an unknown 3D scene approximating its radiance and density fields from a set of known (ground-truth) views by using a multilayer perceptron (MLP). This formulation enables differentiable rendering of unseen views [18]. Because NeRF is designed to optimise its parameters on one scene based on a set of known views, overfitting is likely to occur when the views are few. In general, overfitting can be mitigated via data augmentation, and, to the best of our knowledge, the only method that addresses data augmentation for NeRF is AugNeRF [4]. AugNeRF aims at improving NeRF generalisation by using adversarial data augmentation to enforce each ray and its augmented version to produce the same result. AugNeRF perturbs NeRF at the input coordinates, the intermediate features and the pre-rendering output. We experimentally observed that AugNeRF underperforms NeRF when the known input views are few (e.g. four, eight). Unlike AugNeRF, we do not perturb the known input views, but we instead synthesise new views (novel 3D projective transformations) between pairs of known views.

There exist solutions that specifically target the problem of training NeRF when the input views are few, which are pixelNeRF [28], MVSNeRF [3], and DietNeRF [11]. PixelNeRF [28] and

MVSNerf [3] condition the NeRF’s output through features computed with auxiliary deep networks. During the rendering phase, a feature is processed for each sampled 3D point that is provided as input to the MLP for the conditioning. Unlike these approaches, DVM does not rely on an auxiliary deep network, which has to be trained separately and ad-hoc, to process the known input images. DietNeRF [11] extends NeRF design by extracting feature vectors of the known images through a CLIP pre-trained image encoder. DietNeRF training renders some random poses and processes them using the very same CLIP image encoder. DietNeRF adds a loss component to minimise the cosine distance between CLIP feature vectors of the images rendered from random views and of ground-truth images. Unlike DietNeRF, we do not need an additional consistency loss that is computed through the additional CLIP Vision Transformer to extract semantic representations of renderings, but we instead produce actual images from random viewpoints through view morphing.

3 Preliminaries

3.1 NeRF overview

NeRF’s objective is to synthesise novel views of a scene by optimising a volumetric function given a finite set of input views [18]. Let f_θ be the underlying function we aim to optimise. The input to f_θ is a 5D datum that encodes a point on a camera ray, i.e. a 3D spatial location (x, y, z) and a 2D viewing direction (θ, ϕ) . Let $\mathbf{c} \in \mathbb{R}^3$ be the view-dependent emitted radiance (colour) and σ be the volume density that f_θ predicts at (x, y, z) . Novel views are synthesised by querying 5D data along the camera rays. Traditional volume rendering techniques can be used to transform \mathbf{c} and σ into an image [12, 16]. Because volume rendering is differentiable, f_θ can be implemented as a fully-connected deep network and learned.

Rendering a view from a novel viewpoint consists of estimating the integrals of all 3D rays that originate from the camera optic centre and that pass through each pixels of the camera image plane. Let \mathbf{r} be a 3D ray. To make rendering computationally tractable, each ray is represented as a finite set of 3D spatial locations, which are defined between two clipping distances: a near one (t_n) and a far one (t_f). Let Γ be the number of 3D spatial locations sampled between t_n and t_f . Rendering the colour of a pixel can be performed by computing

$$\hat{\mathbf{c}}(\mathbf{r}) = \sum_{i=1}^{\Gamma} s(i) (1 - e^{-\sigma_i \delta_i}) \mathbf{c}_i, \quad \text{where } s(i) = e^{-\sum_{j=1}^{i-1} \sigma_j \delta_j}, \quad (1)$$

where $s(i)$ is the inverse of the volume density that is accumulated up to the i^{th} spatial location and $(1 - e^{-\sigma_i \delta_i})$ is a density-based weight component: the higher the density value of a point, the larger the contribution on the final rendered colour. $\delta_i = t_{i+1} - t_i$ is the distance between adjacent sampled 3D spatial locations, and \mathbf{c}_i and σ_i are the colour and volume density predicted by NeRF at the i^{th} spatial location.

Rendering a depth value at a given pixel can be performed by substituting \mathbf{c}_i with the distance of the i^{th} spatial location with respect to the camera optic centre, i.e. z_i . Let $\hat{d}(\mathbf{r})$ be the estimated depth value for the ray \mathbf{r} .

The input required to learn NeRF parameters is a set of N images and their corresponding camera information. Let $\mathcal{I} = \{\mathbf{I}_k\}_{k=1}^N$ be the training images, and $\mathcal{P} = \{\mathbf{P}_k\}_{k=1}^N$ and $\mathcal{K} = \{\mathbf{K}_k\}_{k=1}^N$ be their corresponding camera poses and intrinsic parameters, respectively.

Learning f_θ is achieved by comparing each ground-truth pixel $\mathbf{c}(\mathbf{r})$ with its predicted counterpart $\hat{\mathbf{c}}(\mathbf{r})$. Hence, the goal is to minimise the following L2-norm objective function

$$\mathcal{L} = \frac{1}{|\mathcal{R}|} \sum_{\mathbf{r} \in \mathcal{R}} (\|\mathbf{c}(\mathbf{r}) - \hat{\mathbf{c}}_c(\mathbf{r})\|_2^2 + \|\mathbf{c}(\mathbf{r}) - \hat{\mathbf{c}}_f(\mathbf{r})\|_2^2), \quad (2)$$

where $\hat{\mathbf{c}}_c(\mathbf{r})$ and $\hat{\mathbf{c}}_f(\mathbf{r})$ are the coarse and fine predicted volume colours for ray \mathbf{r} , respectively. Please refer to [18] for more details.

3.2 View morphing overview

View morphing objective is to synthesise realistic 2D transitions between an image pair $(\mathbf{I}_k, \mathbf{I}_{k'})$. Firstly, the two images are *prewarped* through rectification, i.e. their image planes are aligned without

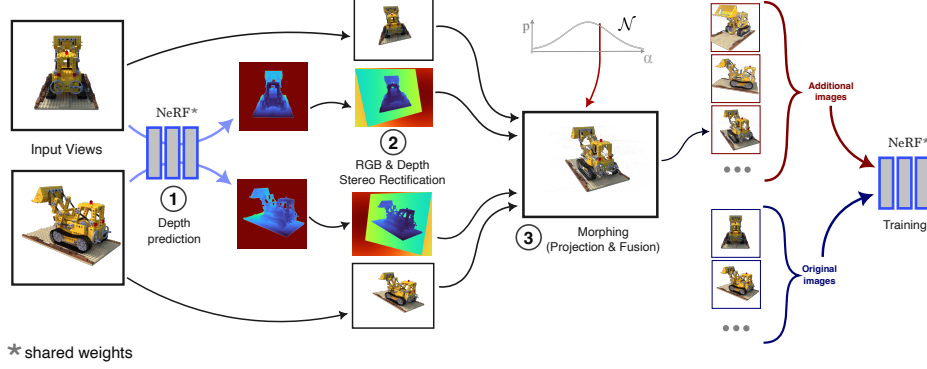


Figure 2: Block diagram of Depth-based View Morphing for NeRF main steps. From the left, we (1) predict the depth with NeRF, (2) rectify the input images and predicted depths, and (3) compute the image morphing of a view randomly positioned between the view pair. α determines the new view position and it is sampled from a Gaussian distribution.

changing their cameras’ optic centres. Secondly, the *morph* is computed between these prewarped images to generate an in-between image whose viewpoint lies on the line connecting the optic centres. Thirdly, the image plane of the in-between image is transformed to a desired viewpoint through *postwarping*.

In practice, assuming the two views are prewarped, the morph requires the knowledge of their camera poses $\mathbf{P}_k, \mathbf{P}_{k'}$, and the pixel correspondence maps between the images, i.e. $q_k : \mathbf{I}_k \Rightarrow \mathbf{I}_{k'}, q_{k'} : \mathbf{I}_{k'} \Rightarrow \mathbf{I}_k$ [22]. Pixel correspondences can be created by a user or by keypoint detectors, subsequently densified via interpolation to create a map. Note that a correspondence may be a one-to-many match. A warp function for each image can be computed from the correspondence map through linear interpolation as

$$\begin{aligned} w_k(\mathbf{m}_k, \alpha) &= (1 - \alpha) \mathbf{m}_k + \alpha q_k(\mathbf{m}_k), \\ w_{k'}(\mathbf{m}_{k'}, \alpha) &= (1 - \alpha) q_{k'}(\mathbf{m}_{k'}) + \alpha \mathbf{m}_{k'}, \\ \mathbf{P}_\alpha &= (1 - \alpha) \mathbf{P}_0 + \alpha \mathbf{P}_1, \end{aligned} \quad (3)$$

where \mathbf{m}_k is a pixel coordinate of image k , $w_k(\mathbf{m}_k, \alpha)$ is a pixel coordinate of the in-between image, and $\alpha \in [0, 1]$ regulates the position of the in-between image along the connecting line. The in-between image \mathbf{I}_α can be computed by averaging the pixel colours of the warped images. Please refer to [23] for more details.

4 Our approach: Depth-based View Morphing for NeRF

The goal of Depth-based View Morphing (DVM) is to synthesise additional training input views $\mathcal{G} = \{\mathbf{G}_k\}_{k=1}^W$ by using the predicted depth of nearby ground-truth view pairs and by linearly interpolating their image content. Because the linear interpolation is computed from corresponding pixels between views, the quality of the predicted depth is key. Therefore, we let NeRF warm up by training on the known views for λ iterations before synthesising and injecting DVM-generated views in the training process.

Fig. 2 shows the sequence of three operations of our data augmentation approach for NeRF after the initial warmup stage. These three steps will be described in the following sections: (i) how we compute the depth, (ii) how we adapt the rectification algorithm proposed by Fusiello et al. [6] to handle NeRF camera configurations, and (iii) how we morph the images given the relative depths.

4.1 Rectification

We use Fusiello et al. [6] algorithm for rectification, as we experimentally observed it can produce rectified images containing most of the photometric information from both the unrectified images. Differently, Hartley and Zisserman’s algorithm [8] produces rectified images whose content is more biased towards one of the two unrectified images. Rectification algorithms are typically based on the

assumptions that viewpoints are aligned horizontally and that the reference viewpoint is the left hand side camera (from an observer positioned behind the cameras). This is not the typical configuration in NeRF, as viewpoints may have arbitrary configurations. In such cases, Fusiello et al. algorithm [6] produces rectified views that are inconsistent with the initial camera poses and in the supplementary material we provide examples where the method [6] fails at rectification. We upgrade [6] in order to handle general stereo configurations by first determining the warping matrices to transform the content of the original images, and then warping the images and the depth maps on a common plane.

Warping matrices. Here the objective is to rotate P_k and $P_{k'}$ around their optic centres until their image planes become coplanar. This step allows us to compute the warping matrices W_k and $W_{k'}$ that we can directly apply to the pixel coordinates of the original images to produce the desired rectification result. Let $\tilde{R}_k = [v_{x,k}^T, v_{y,k}^T, v_{z,k}^T]$ be the rotation matrix that we aim at computing to achieve these rotations. Having image planes coplanar ensures that the baseline belongs to the shared plane and that epipolar lines are parallel. Since the baseline must be parallel to the new x axis of both cameras, we can define it as $v_{x,k} = o_k - o_{k'}$, where o_k is the optic centre of camera k . The new y axis can be defined as the cross product between $v_{x,k}$ and the original camera direction z_k , i.e. $v_{y,k} = v_{x,k} \times z_k$. Note that this operation assumes a specific horizontal stereo configuration, which is the constraint of [6] that we want to generalise. Therefore, we firstly detect the configuration of a specific camera pair (i.e. beyond the horizontal assumption), and then modify the new x and y axes in order to apply [6] correctly, thus producing coherent rectified images.

We assess the camera configuration through the application of four vectors defined in the reference frame of camera k : $a_1 = (1, 1, 0)$, $a_2 = (-1, 1, 0)$, $a_3 = (1, 0, 0)$, and $a_4 = (0, 1, 0)$. We use these vectors to calculate the relative orientation of each camera (with respect to camera k) and thus to determine whether to modify the camera axes

First, we check whether the two cameras are in a vertical configuration by computing

$$s = \left| \frac{a_1 \cdot v_{x,k}}{\|a_1 \cdot v_{x,k}\|} + \frac{a_2 \cdot v_{x,k}}{\|a_2 \cdot v_{x,k}\|} \right|. \quad (4)$$

If $s \neq 0$, $v_{x,k}$ and $v_{y,k}$ are swapped. Then, we evaluate the horizontal configuration, making sure the reference camera is on the left hand side and compute

$$v_{x,k} = v_{x,k} \underbrace{\frac{a_3 \cdot v_{x,k}}{\|a_3 \cdot v_{x,k}\|}}_{\in \{1, -1\}}, \quad v_{y,k} = v_{y,k} \underbrace{\frac{a_4 \cdot v_{y,k}}{\|a_4 \cdot v_{y,k}\|}}_{\in \{1, -1\}}. \quad (5)$$

The new z axis is obtained as $v_{z,k} = v_{x,k} \times v_{y,k}$. We can then compute the warping matrices as

$$W_k = (\tilde{K} \cdot \tilde{R}_k) \cdot (K_k \cdot R_k)^{-1}, \quad W_{k'} = (\tilde{K} \cdot \tilde{R}_k) \cdot (K_{k'} \cdot R_{k'})^{-1}, \quad (6)$$

where $\tilde{K} = \frac{1}{2}(K_k + K_{k'})$ is the matrix of intrinsic parameters. The new camera pose of k is equal to $\tilde{P}_k = [\tilde{R}_k, t_k]$, where t_k is the translation of the original camera pose P_k (same for k').

Image and depth warping. We warp both images and depth maps of both viewpoints k and k' using Eq. 6. Let $\tilde{I}_k = I_k \circ W_k$ be the warped image, where \circ is the operator that warps the pixel coordinates of I_k into the rectified image. If we warp the depth maps in the same way as the images, we would obtain distorted rectified depth maps, therefore we first convert each depth value into its 3D coordinate (in the global reference frame) counterpart by using the camera parameters, resulting in a map of 3D coordinates of the same size as the original depth map. Let D_k be the depth map predicted by NeRF of view k and D_k^{3D} be its 3D coordinate map counterpart. Then, we apply the warping as $\tilde{D}_k^{3D} = D_k^{3D} \circ W_k$ and we transform \tilde{D}_k^{3D} to depth map \tilde{D}_k by using the camera parameters.

4.2 Image morphing

Image morphing fuses the rectified images to obtain the new image for data augmentation during training. We begin by transforming images and depth maps into coloured 3D point clouds. Specifically, we combine \tilde{I}_k and \tilde{D}_k^{3D} to produce the relative coloured point cloud X_k (same for k'). As in Eq. 3, we define the new camera pose as $\tilde{P}_\alpha = (1 - \alpha)\tilde{P}_k + \alpha\tilde{P}_{k'}$, where $\alpha \in [0, 1]$ regulates the position of the new viewpoint between the two original views. We use \tilde{P}_α to transform X_k and $X_{k'}$ in the

local reference system of the new viewpoint. Then, \mathbf{X}_k and $\mathbf{X}_{k'}$ are projected onto the new image plane and if some 3D points are projected on the same pixels, they are fused via coalescence by selecting the nearest one to the camera’s optic centre [2]. We use coalescence for merging pixels because it can be implemented on GPU [13].

4.3 Applying DVM for data augmentation

DVM is subject to the same geometric constraints as the original view morphing technique [23]. These constraints include singular camera configurations, which occur when the optic centre of a camera is within the field of view of another one [23]. We also discard cameras that are distant from each other more than a threshold γ , as the in-between cameras may be on a transition path that cross regions where the object of interest is not visible.

Because view morphing allows the synthesis of a new view at any point on the line that connects the known camera pair, we randomly sample new views using a Gaussian distribution centred half-way through the camera pair. Specifically, if we consider a normalised distance between the two cameras, the Gaussian distribution is centred at 0.5 and the standard deviation σ is chosen such that $3\sigma \rightarrow 0$ at the optic centre positions. Therefore, we sample $\alpha \sim \mathcal{N}(0.5, \sigma)$. For each valid camera pair, we regenerate M new views every η training iterations as the predicted depth improves over time during training.

5 Experiments

5.1 Experimental setup

We evaluate our method on three training setups by using the NeRF realistic synthetic 360° dataset [18], which is composed of eight scenes, i.e. Chair, Drums, Ficus, Lego, Materials, Ship, Mic, Hot, and Dog. **First setup:** We select $N = 8$ views out of 100 available for each scene using the Farthest Point Sampling (FPS) [19] (the first view is used for FPS initialisation in each scene). **Second setup:** we use the same $N = 8$ views used in DietNeRF [11]. **Third setup:** we select $N = 4$ views using the previous FPS approach. We test each trained model on all the test views of NeRF realistic synthetic 360°. We quantify the rendering results using the peak signal-to-noise ratio (PSNR) score, structured similarity index measure (SSIM) [26] and learned perceptual image patch similarity (LPIPS) [29].

We quantitatively compare our approach against DietNeRF [11] as being a recent method for few-shot view synthesis, and against AugNeRF [4] because it is the only data augmentation for NeRF method available, with the difference that it perturbs input while we do new views generation. We also include a qualitative comparison against these methods at the end.

We implement two oracle methods in order to report upper-bound results of DVM. The first oracle method is called *NeRF [18] + oracle image* where we replace the image synthesised with DVM by a ground-truth image rendered from the known 3D object, while the second method is *NeRF [18] + DVM (oracle depth)* where we synthesise with DVM the new image using the ground-truth depth as opposed to the predicted one.

We use the Chair scene for our ablation study, which consist of testing DVM on four different, randomly-chosen, configurations of eight views and on the DietNeRF configuration.

We implement NeRF and our approach in PyTorch Lightning, and run experiments on a single Nvidia A40 with a batch size of 1024 rays. A single scene can be trained in about two days. We use the original implementations of DietNeRF and AugNeRF. We set the same training parameters as in [18], and set $\gamma = 6$, $\sigma = 0.2$, $M = 1$, $\eta = 5K$, $\lambda = 500$.

5.2 Analysis of the results

Tab. 1 shows the results averaged over the eight scenes. Per-scenes results can be found in the supplementary material. Our NeRF implementation can achieve nearly the same results reported in [18] on the 100-view setup, i.e. PSNR equal to 31.21 (ours) compared to 31.01 ([18]). We can observe that when we apply DVM on the eight- and four-view setups, the quality of the NeRF renderings improves. The largest contribution is in the four-view setup where we obtain an improvement of 5.92 PSNR on average. Here, the maximum improvement occurs in the Lego scene where we obtain a

Table 1: Results on the NeRF realistic synthetic 360° dataset.

# views	Method	PSNR \uparrow	SSIM \uparrow	LPIPS \downarrow
100 [18]	NeRF [18]	31.21	0.9513	0.0465
8	NeRF [18] + oracle image	26.14	0.9038	0.0893
	NeRF [18] + DVM (oracle depth)	24.22	0.8800	0.1076
8	NeRF [18]	23.45	0.8673	0.1303
	DietNeRF [11]	22.98	0.8545	0.1258
	AugNeRF [4]	10.04	0.5415	0.3866
	NeRF [18] + DVM	24.39	0.8768	0.1146
8 [11]	NeRF [11]	20.09	0.822	0.179
	DietNeRF [11]	23.59	0.8740	0.0970
	NeRF [18] + DVM	24.14	0.8729	0.1180
4	NeRF [18]	10.98	0.6550	0.3620
	DietNeRF [11]	12.61	0.6591	0.3302
	AugNeRF [4]	8.14	0.3924	0.4802
	NeRF [18] + DVM	16.90	0.7563	0.2461

Table 2: Ablation study. Key. sX: view set X. avg. dist.: average distance between view pairs.

# views	avg. dist.	Method	PSNR \uparrow	SSIM \uparrow	LPIPS \downarrow
8 [11]	5.20	DietNeRF [11]	25.59	0.9120	0.0770
8 [11]	5.20	NeRF + DVM	26.90	0.9180	0.0797
8 (s1)	5.18	NeRF + DVM	27.87	0.9294	0.0693
8 (s2)	4.38	NeRF + DVM	27.13	0.9178	0.0855
8 (s3)	4.73	NeRF + DVM	27.48	0.9317	0.0676
8 (s4)	4.69	NeRF + DVM	28.39	0.9365	0.0598

+10.48 PSNR. However, like DietNeRF, we do not improve in the Ship scene, i.e. we achieve -0.70 PSNR as opposed to -0.91 PSNR of DietNeRF. The results also show that the perturbation of the known input views, done by AugNeRF, has negative effects in all the tested setups.

Fig. 3 shows some qualitative results on Chair, Hot Dog, and Lego, where we can observe that DVM enables NeRF to produce higher definition results than DietNeRF. We speculate that this lack in output details produced by DietNeRF may be due to its CLIP-based approach that is introduced to leverage a semantic consistency loss for regularisation [20]. In fact, the output of CLIP is a low-dimensional (global) representation vector of the image, which may hinder the learning of high-definition details. Differently, our approach interpolates the original photometric information from two views to produce a new input view, without losing information through the encoding of the low-dimensional representation vector. Several more results and analyses can be found in the supplementary material.

Ablation study We assess the stability of DVM by evaluating the rendering quality when different combinations of views are used to train NeRF. Tab. 2 shows that the performance are fairly stable throughout different view configurations. We also observed that the algorithm is robust to variations in the distance between view pairs. As long as a view pair is not singular and the distance between cameras is adequate to create acceptable 3D projective transformations of the object, we can successfully synthesise new views with DVM.

6 Conclusions

We presented a novel data augmentation method for NeRF approaches that is based on the view morphing technique [23]. View morphing requires no prior knowledge of the 3D shape and it is based on general principles of projective geometry. We showed how to synthesise random novel 3D projective transformations of the object between viewpoint pairs using view morphing and how to use them with NeRF. We evaluated our approach on the conventional dataset used by NeRF-based approaches and showed that our data augmentation approach enables NeRF to better learn 3D scenes in different few-shot view synthesis setups. We would like to highlight that DVM is not meant to be a replacement for DietNeRF, or other similar methods, but it is rather a data augmentation method

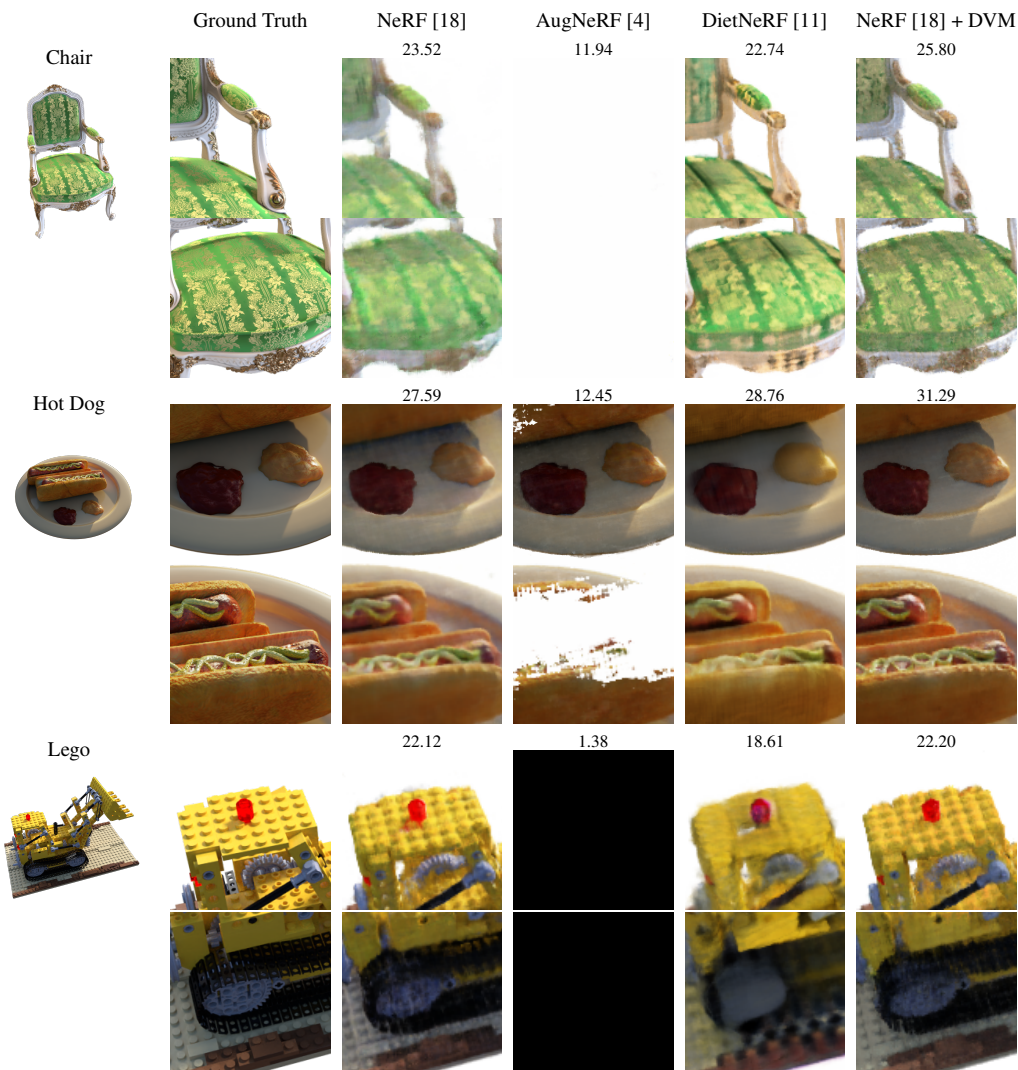


Figure 3: Comparisons on test-set views of scenes of NeRF realistic synthetic 360°. Unlike AugNeRF [4], DVM is an effective data augmentation method that can be used for few-shot view synthesis problems. Unlike DietNeRF [11], DVM enables NeRF to learn scenes with a higher definition. We report the PSNR that we measured for each method and for each rendered image. AugNeRF unsuccessfully learns Chair and Lego (white and black outputs).

that can be used together with any NeRF-based approach. We designed our approach to be fully differentiable, so an attractive research direction is to embed our approach in NeRF and exploit it at the loss level by aggregating photometric information from multiple cameras.

References

- [1] Jonathan T Barron, Ben Mildenhall, Matthew Tancik, Peter Hedman, Ricardo Martin-Brualla, and Pratul P Srinivasan. Mip-nerf: A multiscale representation for anti-aliasing neural radiance fields. In *ICCV*, 2021.
- [2] Gregory J Chaitin. Register allocation & spilling via graph coloring. *ACM Sigplan Notices*, 17(6):98–101, June 1982.
- [3] Anpei Chen, Zexiang Xu, Fuqiang Zhao, Xiaoshuai Zhang, Fanbo Xiang, Jingyi Yu, and Hao Su. MVSNeRF: Fast Generalizable Radiance Field Reconstruction from Multi-View Stereo. In *CVPR*, 2021.

- [4] Tianlong Chen, Peihao Wang, Zhiwen Fan, and Zhangyang Wang. Aug-NeRF: Training Stronger Neural Radiance Fields with Triple-Level Physically-Grounded Augmentations. In *CVPR*, 2022.
- [5] Frederic Devernay and Adrian Ramos Peon. Novel view synthesis for stereoscopic cinema: detecting and removing artifacts. In *Workshop on 3D Video Processing (ACMMM)*, 2010.
- [6] Andrea Fusiello, Emanuele Trucco, and Alessandro Verri. A compact algorithm for rectification of stereo pairs. *Machine Vision and Applications*, 12(1):16–22, Jul 2000.
- [7] Orazio Gallo, Alejandro Troccoli, and Varun Jampani. Novel view synthesis: From depth-based warping to multi-plane images and beyond. Conference on Computer Vision and Pattern Recognition, 2020. URL <https://nvlabs.github.io/nvs-tutorial-cvpr2020/>.
- [8] R. I. Hartley and A. Zisserman. *Multiple View Geometry in Computer Vision*. Cambridge University Press, 2004.
- [9] Peter Hedman, Pratul P. Srinivasan, Ben Mildenhall, Jonathan T. Barron, and Paul Debevec. Baking neural radiance fields for real-time view synthesis. In *ICCV*, 2021.
- [10] Jeffrey Ichnowski, Yahav Avigal, Justin Kerr, and Ken Goldberg. Dex-nerf: Using a neural radiance field to grasp transparent objects. In *CRL*, 2022.
- [11] Ajay Jain, Matthew Tancik, and Pieter Abbeel. Putting NeRF on a Diet: Semantically Consistent Few-Shot View Synthesis. In *ICCV*, 2021.
- [12] J.T. Kajiya and B.P.V. Herzen. Ray tracing volume densities. In *SIGGRAPH*, 1984.
- [13] Varun Kanade, Frederik Mallmann-Trenn, and Thomas Sauerwald. On coalescence time in graphs: When is coalescing as fast as meeting?: Extended Abstract. In *Thirtieth Annual ACM-SIAM Symposium on Discrete Algorithms*, 2019.
- [14] W.E. Lorensen and H.E. Cline. Marching Cubes: A High Resolution 3D Surface Construction Algorithm. In *SIGGRAPH*, 1987.
- [15] Ricardo Martin-Brualla, Noha Radwan, Mehdi S. M. Sajjadi, Jonathan T. Barron, Alexey Dosovitskiy, and Daniel Duckworth. NeRF in the Wild: Neural Radiance Fields for Unconstrained Photo Collections. In *CVPR*, 2021.
- [16] N. Max. Optical models for direct volume rendering. *IEEE Transaction on Visualization and Computer Graphics*, 1(2):99–108, june 1995.
- [17] Ben Mildenhall, Pratul P. Srinivasan, Rodrigo Ortiz-Cayon, Nima Khademi Kalantari, Ravi Ramamoorthi, Ren Ng, and Abhishek Kar. Local light field fusion: Practical view synthesis with prescriptive sampling guidelines. *ACM Transactions on Graphics (TOG)*, 38(29):1–14, august 2019.
- [18] Ben Mildenhall, Pratul P. Srinivasan, Matthew Tancik, Jonathan T. Barron, Ravi Ramamoorthi, and Ren Ng. NeRF: Representing Scenes as Neural Radiance Fields for View Synthesis. In *ECCV*, 2020.
- [19] Charles R Qi, Or Litany, Kaiming He, and Leonidas J Guibas. Deep hough voting for 3d object detection in point clouds. In *ICCV*, 2019.
- [20] Alec Radford, Jong Wook Kim, Chris Hallacy, Aditya Ramesh, Gabriel Goh, Sandhini Agarwal, Girish Sastry, Amanda Askell, Pamela Mishkin, Jack Clark, Gretchen Krueger, and Ilya Sutskever. Learning transferable visual models from natural language supervision. In *ICML*, 2021.
- [21] Johannes Lutz Schönberger and Jan-Michael Frahm. Structure-from-Motion Revisited. In *CVPR*, 2016.
- [22] Steven M Seitz and Charles R Dyer. View morphing. In *Conference on Computer graphics and interactive techniques*, 1996.

- [23] Steven M Seitz and Charles R Dyer. View morphing. In *Conference on Computer graphics and interactive techniques*, 1996.
- [24] Connor Shorten and Taghi M. Khoshgoftaar. A survey on image data augmentation for deep learning. *Journal of Big Data*, 6(1), July 2019.
- [25] A. Tewari and et al. Advances in neural rendering. *Computer Graphics Forum*, 41(2):703–735, May 2022.
- [26] Zhou Wang, A.C. Bovik, H.R. Sheikh, and E.P. Simoncelli. Image quality assessment: from error visibility to structural similarity. *IEEE Transactions on Image Processing*, 13(4):600–612, april 2004.
- [27] Yiheng Xie, Towaki Takikawa, Shunsuke Saito, Or Litany, Shiqin Yan, Numair Khan, Federico Tombari, James Tompkin, Vincent Sitzmann, and Srinath Sridhar. Neural fields in visual computing and beyond. *Computer Graphics Forum*, 41(2):641–676, may 2022.
- [28] Alex Yu, Vickie Ye, Matthew Tancik, and Angjoo Kanazawa. PixelNeRF: Neural radiance fields from one or few images. In *CVPR*, 2021.
- [29] Richard Zhang, Phillip Isola, Alexei A Efros, Eli Shechtman, and Oliver Wang. The unreasonable effectiveness of deep features as a perceptual metric. In *CVPR*, 2018.

Data augmentation for NeRF: a geometric consistent solution based on view morphing

Supplementary material

Matteo Bortolon^{1,2,3} Alessio Del Bue² Fabio Poiesi^{1,2}

¹TeV, Fondazione Bruno Kessler ²PAVIS, Istituto Italiano di Tecnologia

³DISI, University of Trento
{mbortolon,poiesi}@fbk.eu
{alessio.delbue}@iit.it

7 Introduction

The supplementary material is organised as follows.

- Sec. 8 shows quantitative results for each scene of the NeRF realistic synthetic 360° dataset;
- Sec. 9 includes additional qualitative results when eight and four views are used for training;
- Sec. 10 shows two examples of the rectification problem we experienced with Fusiello et al. [6] algorithm;
- Sec. 11 includes an analysis of the depth learned by NeRF.
- Sec. 12 includes some examples of view morphing results produced with DVM that are generated with the depth predicted by NeRF.

8 Quantitative results per scene

We evaluate our method on three training setups by using the NeRF realistic synthetic 360° dataset [18], which is composed of eight scenes, i.e. Chair, Drums, Ficus, Lego, Materials, Ship, Mic, Hot, and Dog. First setup: We select $N = 8$ views out of 100 available for each scene using the Farthest Point Sampling (FPS) (the first view is used for FPS initialisation in each scene). Second setup: we use the same $N = 8$ views used in DietNeRF [11]. Third setup: we select $N = 4$ views using the previous FPS approach. We test each trained model on all the test views of NeRF realistic synthetic 360°. We quantify the rendering results using the peak signal-to-noise ratio (PSNR) score, structured similarity index measure (SSIM) and learned perceptual image patch similarity (LPIPS).

The numerical results for each scene are reported in Tab. 3 for PSNR, Tab. 4 for SSIM, and Tab. 5 for LPIPS. In terms of PSNR, we can see that our approach outperforms the other approaches on almost all the scenes. In terms of SSIM and LPIPS, we can see that our approach is typically on par with NeRF and DietNeRF in the case of 8-views setting. This is mainly due to how these two measures are formulated that are less sensitive to high-frequency variations, but they rather aim at measuring the perceptual similarity between two images. In the case of 4-views setting our approach often outperforms the other approaches as it allows NeRF to correctly learn the geometry of the scene.

9 Additional qualitative results

Figs. 4 and 5 show results of the other scenes that are not shown in the main paper. In these examples we can see how the proposed method enables NeRF to improve the quality of the learned scenes.

Table 3: PSNR metric per-scene results on the NeRF realistic synthetic 360° dataset.

# views	Method	Chair	Drums	Ficus	Hot Dog	Lego	Materials	Mic	Ship
100	<i>NeRF [18]</i>	34.57	25.71	29.05	36.88	31.47	29.49	33.05	29.48
8	NeRF [18] + oracle image	29.91	21.65	21.98	31.42	26.72	23.35	28.95	25.14
	NeRF [18] + DVM (oracle depth)	28.39	21.13	21.95	27.05	23.76	21.12	27.00	23.37
8	NeRF [18]	25.11	19.93	21.72	23.19	24.65	21.95	27.81	23.27
	DietNeRF [11]	26.01	18.79	20.89	26.01	21.55	21.28	27.32	21.99
	AugNeRF [4]	15.05	0.75	14.86	12.50	1.04	9.94	13.40	12.81
	NeRF [18] + DVM	27.87	20.20	21.36	27.15	24.84	22.35	27.61	23.71
4	NeRF [18]	14.11	10.45	14.29	10.35	9.38	8.28	13.13	7.85
	DietNeRF [11]	19.88	9.84	17.77	9.99	8.97	16.43	11.04	6.94
	AugNeRF [4]	13.57	11.18	14.16	1.05	9.82	1.12	11.94	2.27
	NeRF [18] + DVM	22.49	16.71	18.68	10.84	19.86	18.72	20.79	7.15

Table 4: SSIM metric per-scene results on the NeRF realistic synthetic 360° dataset.

# views	Method	Chair	Drums	Ficus	Hot Dog	Lego	Materials	Mic	Ship
100	<i>NeRF [18]</i>	0.9790	0.9288	0.9627	0.9785	0.9610	0.9557	0.9753	0.8694
8	NeRF [18] + oracle image	0.9505	0.8748	0.8789	0.9606	0.9129	0.8870	0.9625	0.8031
	NeRF [18] + DVM (oracle depth)	0.9418	0.8631	0.8753	0.9249	0.8633	0.8420	0.9498	0.7796
8	NeRF [18]	0.8829	0.8320	0.8720	0.8894	0.8820	0.8561	0.9540	0.7696
	DietNeRF [11]	0.9079	0.8020	0.8664	0.9101	0.8033	0.8453	0.9496	0.7515
	AugNeRF [4]	0.7576	0.0004	0.7760	0.7480	0.0012	0.6653	0.7497	0.6340
	NeRF [18] + DVM	0.9294	0.8302	0.8650	0.9266	0.8790	0.8576	0.9508	0.7758
4	NeRF [18]	0.8156	0.5657	0.8207	0.6507	0.5765	0.4765	0.8427	0.4912
	DietNeRF [11]	0.8130	0.5231	0.8195	0.6416	0.5249	0.7632	0.7187	0.7264
	AugNeRF [4]	0.6669	0.5330	0.7340	0.0009	0.5459	0.0008	0.6563	0.0011
	NeRF [18] + DVM	0.8439	0.7327	0.8247	0.7237	0.7737	0.7953	0.8819	0.4744

In particular, in Fig. 5 we can see how DVM allows NeRF to learn the correct geometry of the scenes Mic, Lego, and Drums, as opposed to DietNeRF where it instead fails. Ship and Hot Dog are challenging scenes that all the methods fail to learn correctly.

10 Rectification problem

Rectification algorithms are typically based on the assumptions that viewpoints are aligned horizontally and that the reference viewpoint is the left hand side camera (from an observer positioned behind the cameras). This is not the case in NeRF as viewpoints may have arbitrary configurations. For this reason, Fusiello et al. [6] algorithm produces rectified views that are inconsistent with the initial camera poses. We upgrade the algorithm [6] in order to handle general stereo configurations.

Fig. 6 shows the application of [6] to two stereo configurations where the reference viewpoint is (i) the right-hand side camera (horizontal configuration), and (ii) the top camera (vertical configuration). Here, we can observe that when the algorithm in [6] is applied as is the 2D transitions are incorrectly flipped. Instead, if we use our algorithm, the 2D transitions are consistent with starting camera poses.

11 Analysis of the learnt depth

Fig. 7 shows qualitative results about the quality of the learned geometry on the Chair and Lego scenes. We produced the meshed 3D reconstructions by using the marching cubes algorithm [14]. We also include the predicted depth next to each result. As we can observe from the results, the addition of the data augmentation produced by DVM can significantly improve the estimated geometry of the scene.

12 Examples of images produced with DVM

Fig. 8 shows examples of view morphing results produced with DVM that are generated with the depth predicted by NeRF. We generated new views by using the following values of $\alpha = 0.08, 0.23, 0.58$,

Table 5: LPIPS metric per-scene results on the NeRF realistic synthetic 360° dataset.

# views	Method	Chair	Drums	Ficus	Hot Dog	Lego	Materials	Mic	Ship
100	<i>NeRF [18]</i>	<i>0.0225</i>	<i>0.0621</i>	<i>0.0339</i>	<i>0.0286</i>	<i>0.0347</i>	<i>0.0356</i>	<i>0.0254</i>	<i>0.1295</i>
8	NeRF [18] + oracle image	0.0512	0.1067	0.1128	0.0498	0.0690	0.0830	0.0362	0.2060
	NeRF [18] + DVM (oracle depth)	0.0569	0.1139	0.1242	0.0862	0.1131	0.1151	0.0520	0.1994
8	NeRF [18]	0.1286	0.1623	0.1225	0.1380	0.0962	0.1197	0.0505	0.2247
	DietNeRF [11]	0.0857	0.1696	0.1029	0.1039	0.1638	0.1006	0.0473	0.2323
	AugNeRF [4]	0.2871	0.6423	0.2416	0.3042	0.6556	0.3360	0.3064	0.3195
	NeRF [18] + DVM	0.0693	0.1672	0.1243	0.0795	0.0985	0.1144	0.0657	0.1980
4	NeRF [18]	0.2267	0.4545	0.1822	0.4125	0.4285	0.4977	0.1967	0.4971
	DietNeRF [11]	0.1676	0.4652	0.1477	0.4094	0.4481	0.1879	0.3150	0.5009
	AugNeRF [4]	0.3820	0.4684	0.3016	0.6024	0.4561	0.6102	0.3875	0.6336
	NeRF [18] + DVM	0.1628	0.2657	0.1575	0.3527	0.1936	0.1771	0.1696	0.4899

and 0.82. The images include partial views of the object of interest because we feed NeRF with the rectified views directly. These are novel views that help NeRF to better generalise in the case of few-shot view synthesis.

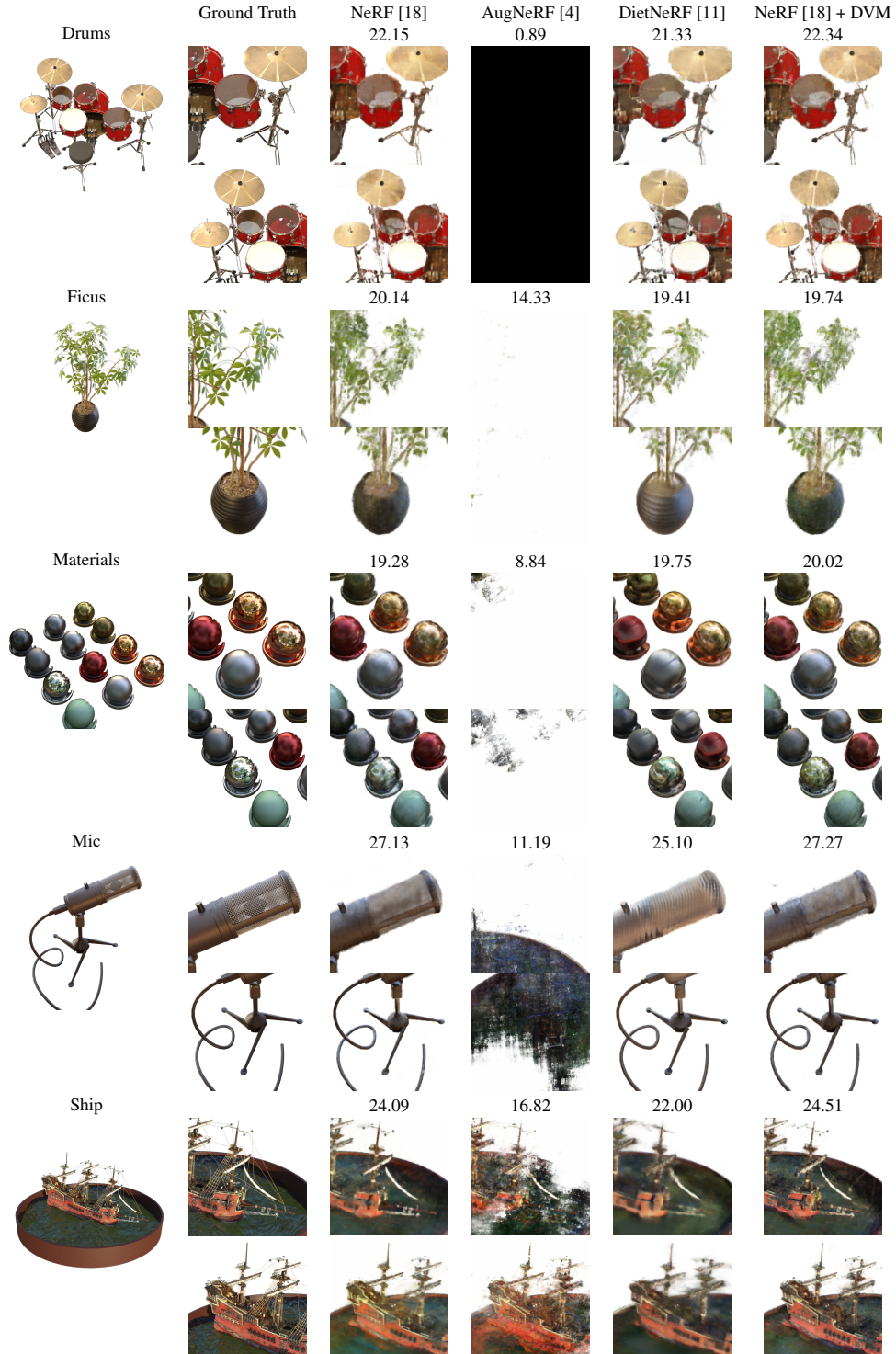


Figure 4: Comparisons on test-set views of scenes of NeRF realistic synthetic 360°, trained on 8-views. Unlike AugNeRF [4], DVM is an effective data augmentation method that can be used for few-shot view synthesis problems. Unlike DietNeRF [11], DVM enables NeRF to learn scenes with a higher definition. We report the PSNR that we measured for each method and for each rendered image.















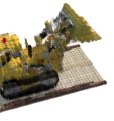












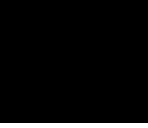



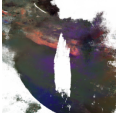





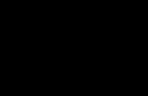


	Ground Truth	NeRF [18] 11.99	AugNeRF [4] 11.92	DietNeRF [11] 19.11	NeRF + DVM 21.41
Chair					
		11.99	11.92	10.87	20.06
Mic					
		7.82	7.62	6.82	18.18
Lego					
		10.84	10.63	10.5	17.11
Drums					
		13.92	13.22	17.17	17.04
Ficus					
		8.28	1.35	14.95	15.4
Materials					
		8.21	2.13	5.88	6.17
Ship					
		8.76	1.69	7.08	7.47
Hot Dog					

Figure 5: Comparisons on test-set views of scenes of NeRF realistic synthetic 360°, trained on 4-views. Unlike other techniques DVM help to increase the probability of building a consistent implicit representation with very sparse view. We report the PSNR that we measured for each method and for each rendered image.

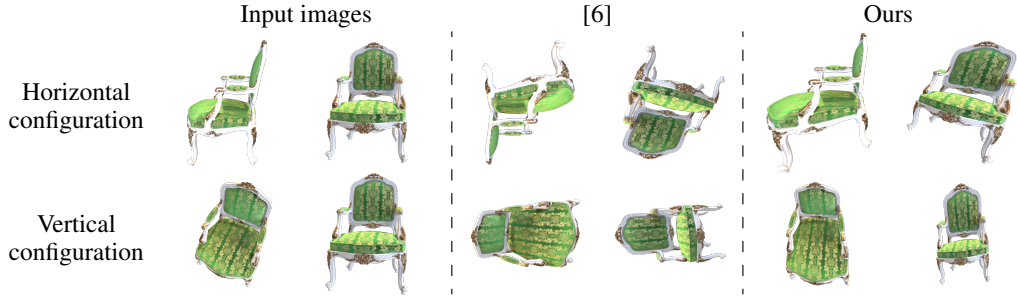


Figure 6: Cases where the algorithm in [6] fails to produce rectification results that are consistent with the original camera configuration.

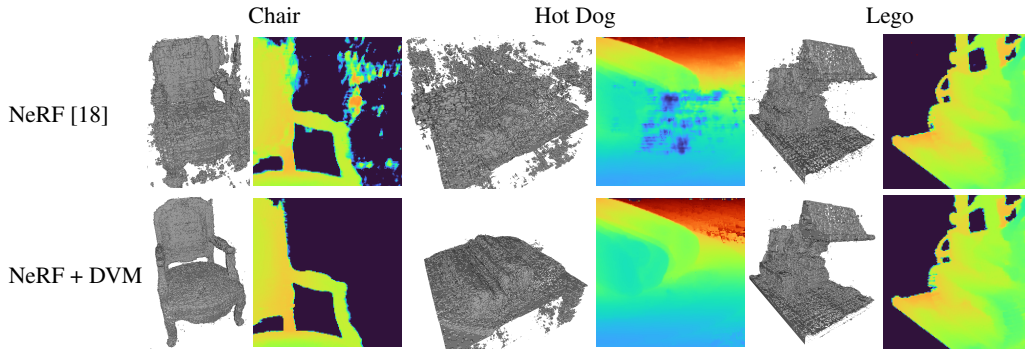


Figure 7: Qualitative comparison between the geometry predicted by NeRF [18] and by NeRF plus our data augmentation DVM. NeRF + DVM leads to smoother and more accurate 3D models.

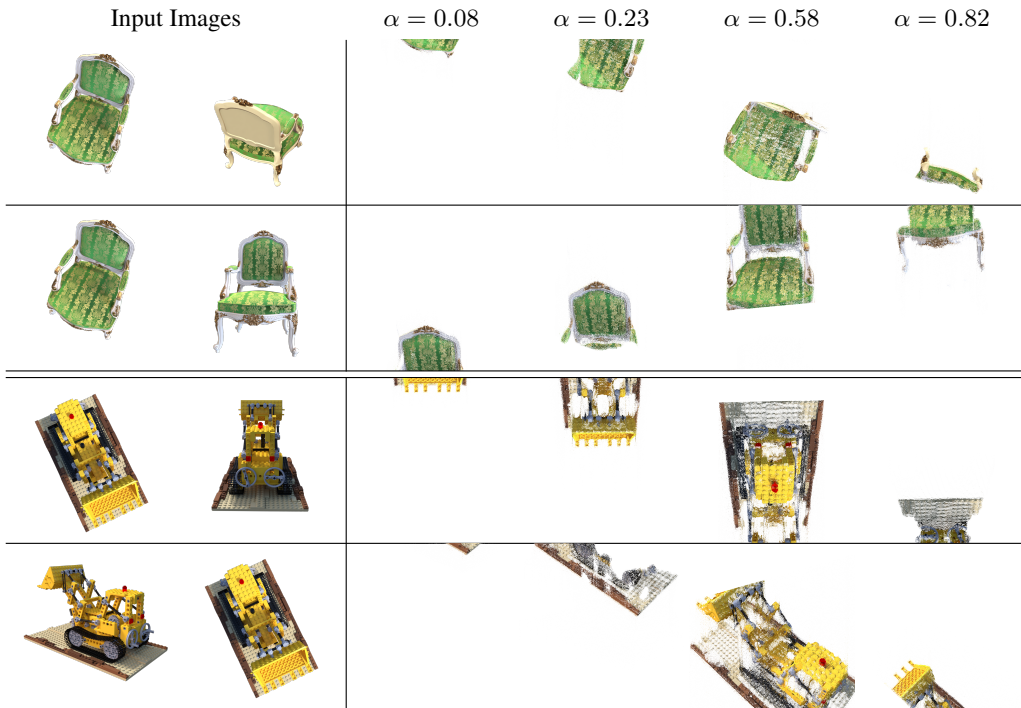


Figure 8: Examples of images generated by DVM using the depth predicted by NeRF.